Journal of
Polymer Materials

Tech Science Press

https://doi.org/10.32604/jpm.2026.077831

ARTICLE

Surface-Functionalized ZnO Nanorods via PEG-Assisted Stabilization for Durable Antibacterial Lyocell Fibers

Biao Liu[1], Xin Wei[1], Zexin Lin[1], Peiyu Cui[1], Junlong Yao[1], Xiaobo Ye[2], Bin Fang[2], Yani Guo[1,*] and Yimin Sun[1,*]

[1]Hubei Key Laboratory of Plasma Chemistry and Advanced Materials, School of Materials Science and Engineering, Wuhan Institute of Technology, Wuhan, China
[2]Dangyang Hongyang New Material Technology Co., Ltd., Dangyang, China

*Corresponding Authors: Yani Guo. Email: guoyni@163.com; Yimin Sun. Email: ymsun@wit.edu.cn

Received: 17 December 2025; Accepted: 22 February 2026; Published: 30 June 2026

ABSTRACT: This study reports a polyethylene glycol (PEG)-assisted surface functionalization strategy to achieve colloidal stabilization of rod-shaped ZnO nanorods and their uniform integration into Lyocell fibers via dry-jet wet spinning. ZnO nanorods are prone to aggregation due to high surface energy, limiting their antibacterial efficacy. We demonstrate that PEG molecules adsorb onto ZnO surfaces through hydrogen bonding and coordination, providing steric stabilization that prevents agglomeration and ensures homogeneous dispersion in the spinning dope. The optimized composite fiber with 3 wt% ZnO exhibits balanced performance, delivering inhibition rates above 95% against *Escherichia coli* and *Staphylococcus aureus*, while retaining over 80% efficacy after 50 laundering cycles. Morphological and structural analyses confirm that PEG-mediated interfacial interactions facilitate stable nanoparticle encapsulation without disrupting the cellulose crystalline structure. Antibacterial mechanism studies further reveal that light-induced reactive oxygen species (ROS) generation is the dominant antibacterial pathway, while Zn^{2+} release provides a secondary contribution. In addition, the antibacterial performance remains stable under different humidity conditions (30%–80% RH), indicating good environmental robustness. This work demonstrates a scalable and eco-friendly route to fabricate durable antibacterial fibers and highlights the broader significance of colloidal stabilization and interfacial engineering in functional polymer composites.

KEYWORDS: Surface functionalization; ZnO nanorods; lyocell fibers; antibacterial durability; ROS generation

1 Introduction

With the growing global concerns about public health and the rising demand for high-performance consumer products, functional textiles that offer both protective performance and eco-friendly properties have attracted significant attention. Lyocell is a regenerated cellulose fiber well known for its renewable biomass origin, closed-loop N-methylmorpholine-N-oxide (NMMO) process, high moisture absorption, and biodegradability [1–5]. However, its hydrophilic and porous nature makes it susceptible to microbial colonization, which compromises durability and hygiene [6,7]. To address this limitation, numerous antibacterial modifications have been explored, including organic biocides, natural extracts, and inorganic nanomaterials [8]. Organic compounds, such as quaternary ammonium salts and chitosan, can rapidly disrupt microbial cell membranes via electrostatic interaction. However, their poor thermal stability, leaching tendencies, and potential to induce resistant strains limit their long-term efficacy [9,10]. Natural extracts, including tea tree oil and aloe vera, offer good biocompatibility, yet their narrow antibacterial spectrum (often

limited to Gram-positive bacteria) and low photothermal stability hinder their industrial scalability [11,12]. In contrast, inorganic agents, particularly ZnO nanoparticles have attracted particular attention due to their broad-spectrum antibacterial activity, thermal stability, and safety profile [13,14].

Recent studies show that particle morphology strongly influences antibacterial performance. Rod-shaped ZnO, with a high aspect ratio and large surface area, offers more active sites for bacterial contact and facilitates photocatalytic ROS generation, leading to enhanced bactericidal efficiency compared with spherical ZnO [15–19]. However, from a colloidal perspective, one of the critical challenges in utilizing ZnO nanorods is their dispersion stability. Due to their high surface energy and anisotropic morphology, ZnO nanorods tend to agglomerate in aqueous or polymeric media, which severely limits their antibacterial efficiency and hinders practical applications [20–22]. Achieving homogeneous dispersion of ZnO nanorods is essentially a colloidal stabilization problem, in which surface modification and interfacial engineering play decisive roles. Polyethylene glycol (PEG) is known to provide steric hindrance and hydrogen bonding interactions with metal oxide surfaces, thereby preventing aggregation and ensuring long-term dispersion stability [23–25]. This steric stabilization mechanism, extensively discussed in colloid and interface science, can be effectively applied to ZnO nanorods to achieve uniform dispersion in polymer matrices. During melt blending, rod-shaped ZnO nanoparticles can also align preferentially along the fiber axis, forming a continuous antibacterial network within the fiber structure. As a result, the antibacterial performance is significantly enhanced [26,27].

In this work, we report a PEG-assisted ultrasonic dispersion strategy to integrate rod-shaped ZnO nanorods into Lyocell fibers via dry-jet wet spinning. Particular emphasis is placed on the interfacial interaction between PEG and ZnO nanorods, which governs their dispersion stability and subsequent antibacterial performance. We demonstrate that PEG not only stabilizes ZnO nanorods through steric repulsion but also facilitates their homogeneous distribution and strong interfacial binding within the Lyocell matrix. The structure–property–function relationships are systematically investigated, highlighting the critical role of colloidal stabilization and surface interactions in achieving durable antibacterial fibers.

2 Experimental Section

2.1 Materials

Dissolving-grade wood pulp and NMMO (50 wt% in H_2O) were supplied by Dangyang Hongyang New Material Technology Co., Ltd. Propyl gallate (PG, purity ≥ 98.5%) was purchased from Shanghai Macklin Biochemical Co., Ltd. ZnO nanorods (purity ≥ 99%, diameter: 30–50 nm, length: 80–150 nm) were provided by Top Metal Materials Co., Ltd. Polyethylene glycol (PEG, Mw ≈ 600) and other analytical-grade chemicals were obtained from Sinopharm Chemical Reagent Co., Ltd.

2.2 Preparation of ZnO/Lyocell Composite Fibers

ZnO nanorods were dispersed in a 6 wt% PEG aqueous solution via ultrasonication (20 kHz, 400 W, 30 min, room temperature) to prevent agglomeration. The dispersion mechanism of ZnO nanorods in the presence of PEG is illustrated in Scheme 1. In this system, PEG molecules anchor to ZnO surfaces via hydrogen bonds (between oxygen atoms and hydroxyl groups), coordination bonds (between oxygen atoms and zinc ions), and physical adsorption (van der Waals forces), while their extended polymer chains generate steric repulsion, effectively inhibiting nanoparticle aggregation and ensuring a uniform distribution in the spinning dope [28].

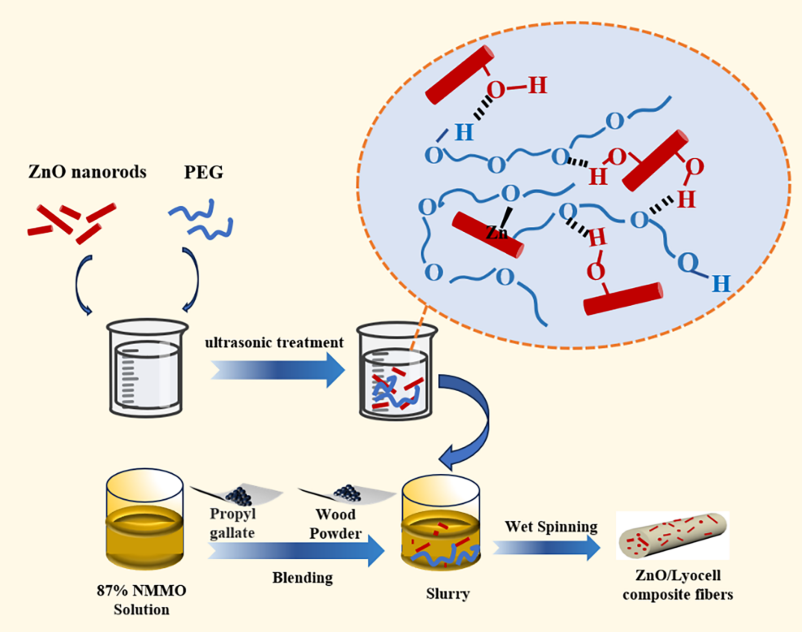

Scheme 1: Schematic illustration of the fabrication process for ZnO/Lyocell composite fibers.

The NMMO aqueous solution (50 wt%) was concentrated to 87 wt% at 110°C under reduced pressure. Subsequently, wood pulp and the ZnO/PEG dispersion were successively added and stirred at 120°C for 2 h to obtain a homogeneous spinning dope. The dope was processed via a dry-jet wet spinning technique: extruded through a spinneret with 12 orifices (orifice diameter: 0.095 mm), passed through a 50 mm air gap, and solidified in a 25 wt% NMMO aqueous solution. The as-spun fibers were thoroughly washed with deionized water to remove residual solvent and dried under vacuum at 60°C. Samples with ZnO loadings of 0, 1.0, 2.0, 3.0, 4.0, and 5.0 wt% were denoted as T-0, T-1, T-2, T-3, T-4, and T-5, respectively. The preparation process is shown in Scheme 1. All spinning parameters were kept constant for all samples.

2.3 Characterization

Morphology was observed using SEM (JSM-5510LV, JEOL, Japan). FTIR (Nicolet iS10, Thermo Fisher Scientific, USA) was used to analyze chemical structures (400–4000 cm^{-1}). Meanwhile, X-ray photoelectron spectroscopy (XPS, K-Alpha, Thermo Fisher Scientific, USA) was utilized to investigate the types of chemical bonding interactions between ZnO nanoparticles, Lyocell fibers and polyethylene glycol (PEG). XRD (D8 ADVANCE, Bruker, Germany) with Cu Kα radiation (λ = 0.15418 nm) characterized crystalline structures. Thermal stability was evaluated via TGA (TGA2, Mettler, Switzerland) from 30°C to 600°C at 10°C/min under N_2 atmosphere. Tensile properties were measured using an electronic universal testing machine (HY0350, China) at 10 mm/min with a span length of 50 mm. Live/dead bacterial staining was visualized via laser scanning confocal microscopy (LSM 800, Carl Zeiss AG, Germany), and bacterial morphology was examined by TEM (JEM-2100, JEOL Ltd., Japan). A 300 W solar-simulated xenon lamp was used as the light source for antibacterial experiments, and the irradiation intensity at the sample surface was maintained at 50 mW/cm^2. For reactive oxygen species (ROS) detection, 5,5-dimethyl-1-pyrroline N-oxide (DMPO) was employed as a superoxide radical trapping agent, and the generated radicals were analyzed using an electron paramagnetic resonance (EPR) spectrometer (EMX PLUS, Bruker, Germany). Briefly, 10 mg of T-3 composite fibers was dispersed in 10 mL of methanol under vigorous stirring. Subsequently, 0.1 mL of the dispersion

was mixed with 0.1 mL of DMPO solution (10 mM). The mixture was then irradiated using the same xenon lamp source (50 mW/cm^2) for 5 min, followed by EPR measurement at 25°C.

2.4 Antibacterial Performance Evaluation

Antibacterial activity against *E. coli* (ATCC 25922) and *S. aureus* (ATCC 6538) was assessed using the colony counting method, zone of inhibition assay, and live/dead fluorescence staining according to standard protocols [29]. Unless otherwise stated, antibacterial experiments were performed under simulated solar light irradiation using a xenon lamp with an incident intensity of 50 mW/cm^2. For dark control experiments, all procedures were conducted under identical conditions except that the samples were fully shielded from light.

2.4.1 Colony Counting Method

Bacterial suspensions (10^6 CFU/mL) were prepared according to standard microbiological procedures [30]. Fiber samples (0.5 g) were first sterilized by UV irradiation for 30 min to eliminate surface contamination. Subsequently, the samples were immersed in 10 mL of bacterial suspension and incubated at 37°C for 18 h under continuous shaking and simulated solar light irradiation (xenon lamp, 50 mW/cm^2), unless otherwise specified. The antibacterial rate (Y, %) was calculated by Formula (1) [31]:

$$Y = \frac{W_T - W_Q}{W_T} \times 100\% \quad (1)$$

where W_T and W_Q are the bacterial colonies on pristine Lyocell and ZnO/Lyocell composite fibers, respectively.

2.4.2 Zone of Inhibition Assay

Bacterial suspensions (~10^9 CFU/mL) were spread evenly on agar plates. UV-sterilized fiber discs (diameter: 1 cm) were placed in the center and incubated at 37°C for 24 h to observe inhibition zones.

Bacterial suspensions (~10^9 CFU/mL) were uniformly spread onto agar plates. UV-sterilized fiber discs (diameter: 1 cm) were placed at the center of the plates, followed by incubation at 37°C for 24 h under simulated solar light irradiation (xenon lamp, 50 mW/cm^2) to observe inhibition zones.

2.4.3 Live/Dead Bacterial Staining

Live/dead bacterial staining was performed using SYTO9 and propidium iodide (PI) [32]. After xenon lamp irradiation (50 mW/cm^2, 5 min), 100 mg of composite fibers was incubated with a mixed solution containing 5 mL of bacterial suspension (10^8 CFU/mL) and 5 mL of 1× PBS for 12 h under shaking. The bacteria were then collected by centrifugation and washed three times with PBS. Subsequently, 100 μL of SYTO9 solution (10 μg/mL) and 100 μL of PI solution (10 μg/mL) were added to the bacterial suspension and incubated in the dark for 40 min. After removing excess dyes by PBS washing, the stained samples were observed using laser scanning confocal microscopy (LSCM).

2.5 Durability of Antibacterial Activity

For the washing durability test, 1 g of fiber sample was immersed in 100 g of an aqueous sodium dodecyl sulfate (SDS) solution (2 wt%) and magnetically stirred at 25°C for 10 min. The fiber was then removed and rinsed with deionized water at 25°C for 1 min, followed by drying in a vacuum oven at 60°C for 24 h.

This procedure was defined as one washing cycle. After each washing cycle, the fibers were subjected to antibacterial tests to evaluate the retention of antibacterial performance.

3 Results and Discussion

3.1 Morphology and Composition Analysis

Fig. 1 shows SEM images of ZnO/Lyocell composite fibers containing 0–5 wt% ZnO. Raw Lyocell fibers exhibit a smooth surface with diameter of about 12 μm (Fig. 1a). For 1 wt%, 2 wt% and 3 wt% ZnO/Lyocell fibers, the surface remains relatively smooth (Fig. 1b–d), indicating ZnO nanoparticles are well dispersed. This highlights the critical role of PEG in providing steric stabilization and interfacial compatibility between ZnO surfaces and the cellulose matrix. As shown in Scheme 1, PEG adsorbs strongly onto ZnO nanorods via hydrogen bonding with surface –OH groups and coordination with unsaturated Zn^{2+} sites [24], this point will be verified in subsequent sections. The extended PEG chains generate a steric barrier that replaces van der Waals-driven aggregation with dominant steric repulsion, suppressing the nanorods' high surface energy–induced clustering [28]. This steric stabilization ensures the colloidal stability of the spinning dope and enables the uniform nanorod dispersion observed in SEM. To further verify the effect of PEG on ZnO dispersion, comparative SEM images of composite fibers with identical ZnO loading (3 wt%) prepared with and without PEG are provided in the Supplementary Information (Fig. S1). The PEG-assisted sample exhibits a more uniform distribution of ZnO nanorods, whereas obvious nanoparticle agglomeration is observed in the absence of PEG, confirming the critical role of PEG in improving dispersion stability. With the increasing of ZnO contents, the fibers surface gradually becomes rough. For 4 wt% and 5 wt% ZnO/Lyocell, surface grooves and protrusions became evident. Especially, at 5 wt% ZnO, obvious aggregation is observed under higher magnification (Fig. S2), suggesting that steric repulsion from PEG chains is insufficient to fully counterbalance van der Waals attraction between nanoparticles. Such concentration-dependent dispersion behavior is consistent with classical colloid stabilization theory, in which the balance between attractive and repulsive interparticle forces determines the state of aggregation. Hence, 3 wt% addition of ZnO ensures uniform dispersion while avoiding particle aggregation, representing the optimal loading. To verify ZnO loading on Lyocell fibers, EDS elemental mapping was performed on the T-1 sample. The C, O, and Zn distributions shown in Fig. 1g,h clearly confirm the immobilization of ZnO on the fiber surface.

The FTIR spectra of Lyocell fibers and various ZnO/Lyocell fibers are presented in Fig. 2a. Characteristic absorption bands at 3354 and 894 cm^{-1} correspond to the stretching vibrations of –OH groups. Peaks at 2899 and 1370 cm^{-1} are attributed to the vibrations of CH_2 and CH moieties in Lyocell fiber, respectively [33,34]. Fig. 2b is an enlarged view of FTIR spectra from 430–630 cm^{-1}, where new weak peaks appear at 440 and 501 cm^{-1} for ZnO/Lyocell composite fibers, attributed to the stretching vibrations of Zn-O [35]. This confirms the presence of nano-ZnO in the composite fibers. The adsorption of PEG chains onto ZnO surfaces likely mediates hydrogen bonding with cellulose hydroxyl groups, thereby facilitating interfacial compatibility.

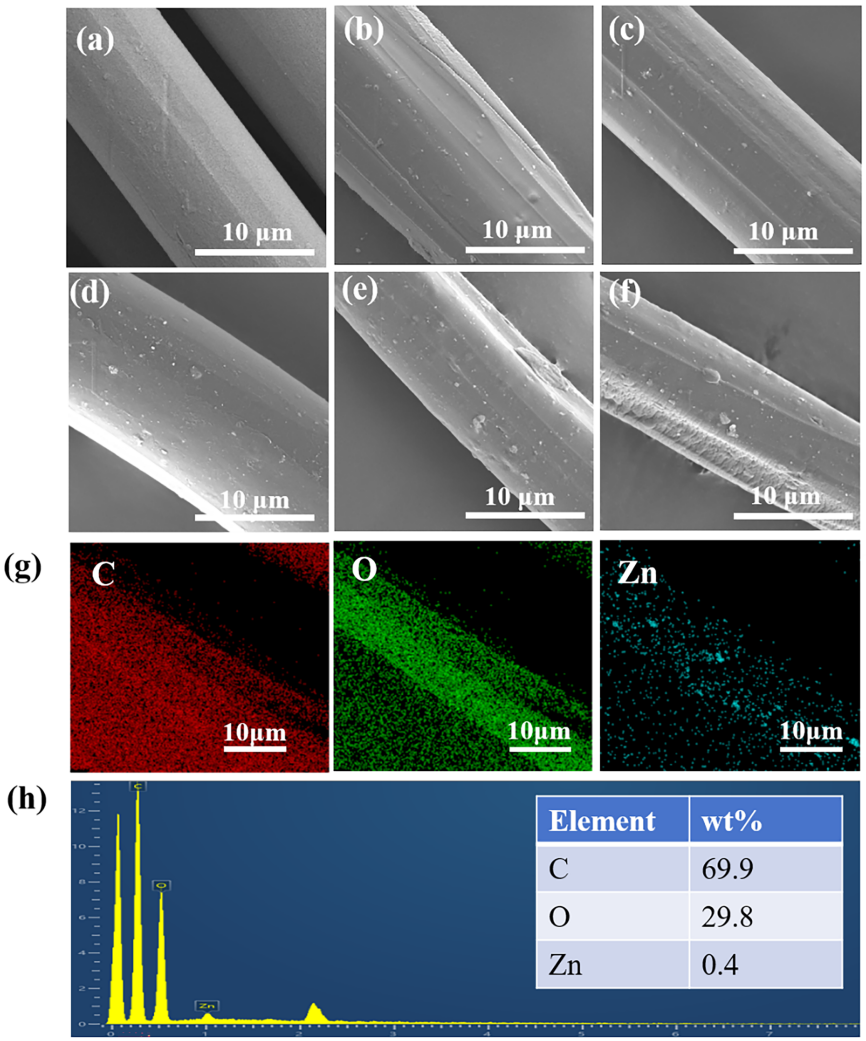

Figure 1: SEM images of composite fibers with varying ZnO loadings: (**a**) T-0, (**b**) T-1, (**c**) T-2, (**d**) T-3, (**e**) T-4, and (**f**) T-5. (**g**) EDS spectrum and (**h**) elemental maps of Zn, C, and O for the T-1 fiber.

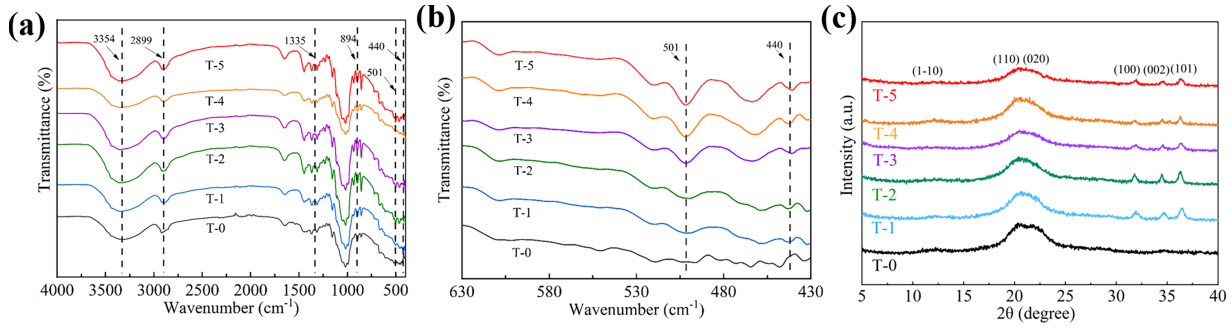

Figure 2: (**a**,**b**) FTIR spectra of ZnO/Lyocell fibers, (**c**) XRD patterns of ZnO/Lyocell fibers.

Fig. 2c presents the XRD patterns of pristine Lyocell fibers and ZnO/Lyocell composites. All samples exhibit characteristic diffraction peaks at 2θ = 12.2°, 20.3°, and 21.4°, which corresponds to the (1-10), (110),

and (020) planes of cellulose crystal type II, indicating that the incorporation of ZnO nanoparticle does not change the crystalline structure of the Lyocell matrix, and the stabilization mechanism is dominated by interfacial interactions rather than lattice incorporation [36,37]. This observation underscores that PEG-mediated colloidal stabilization enables ZnO to be uniformly embedded in the fiber without altering the bulk crystalline framework of cellulose. At low ZnO loadings (≤3 wt%), only a slight reduction in Lyocell diffraction peak intensity is observed in high-resolution XRD patterns, indicating a minor influence on crystallinity and molecular orientation. In contrast, further increasing ZnO content (≥4 wt%) leads to a more evident decrease in peak intensity, suggesting enhanced lattice disturbance and restricted chain alignment during spinning. In addition, all ZnO/Lyocell composites fibers display distinct diffraction peaks at $2\theta = 31.5°$, 34.4°, and 36.5°, which are attributable to the (100), (002), and (101) planes of crystalline ZnO [38]. These results are consistent with SEM observations and further confirm the successful and stable incorporation of ZnO nanoparticles into the Lyocell fiber matrix.

To further investigate the interfacial chemical interactions between PEG and ZnO nanorods, XPS analysis spectra of T-0 and T-3 composite fibers were performed, as shown in Fig. 3.

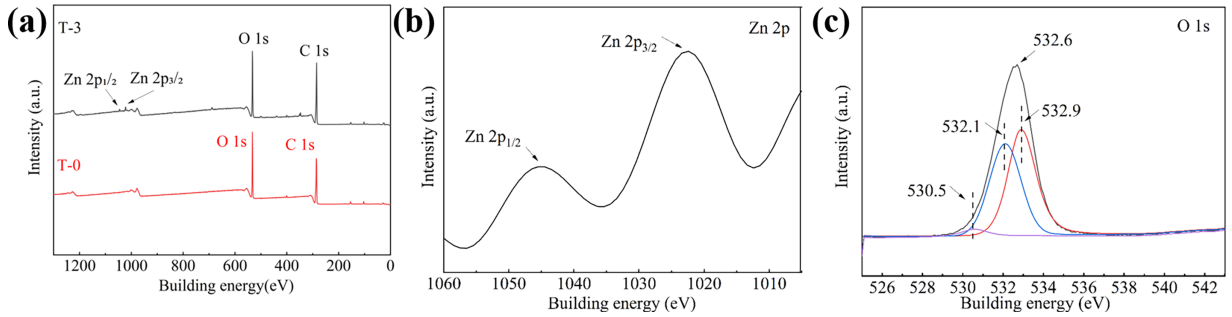

Figure 3: XPS survey spectrum of (**a**) T-0 and T-3, Corresponding high-resolution XPS spectra of T-3: (**b**) high-resolution Zn 2p spectrum, and (**c**) deconvoluted O 1s spectrum.

The Zn 2p spectrum of the composite fibers exhibits two characteristic peaks at binding energies of 1022.4 eV (Zn $2p_3/_2$) and 1045.4 eV (Zn $2p_1/_2$). Compared with the reported values of pristine ZnO, both peaks show a positive shift of approximately 0.6 eV, indicating a modification of the electronic environment of surface Zn^{2+} species. This shift is attributed to coordination interactions between Zn^{2+} ions and the electron-donating oxygen atoms in the ether groups of PEG chains [39]. The high-resolution O 1s spectrum can be deconvoluted into three components centered at 530.5 eV, 532.1 eV, and 532.9 eV. The peak at 530.5 eV corresponds to lattice oxygen in ZnO, while the component at 532.1 eV is assigned to surface hydroxyl oxygen species. The additional component at 532.9 eV is attributed to oxygen species involved in PEG–ZnO interfacial interactions [40]. Compared with typical ZnO surfaces, the relative intensity of the surface hydroxyl oxygen peak is reduced, suggesting that a fraction of surface hydroxyl groups participates in hydrogen bonding with PEG molecules. Moreover, the emergence of the new O 1s component at 532.9 eV provides direct spectroscopic evidence for PEG-related interfacial bonding, confirming the coexistence of coordination interactions and hydrogen bonding at the ZnO–PEG interface. These synergistic interfacial interactions promote stable anchoring of PEG molecules on ZnO nanorod surfaces, which is essential for improving dispersion stability and interfacial compatibility within the Lyocell matrix.

3.2 Mechanical and Thermal Analysis

Fig. 4a,b and Table S1 present the stress-strain curves and elongation at break for Lyocell fibers and composite fibers with varying ZnO contents. The pristine fibers exhibit a tensile strength of approximately

260 MPa and an elongation at break of 6.0%. With increasing ZnO content, both the tensile strength and elongation at break of the composite fibers gradually decline. For 3 wt% ZnO (T-3), the tensile strength and elongation at break are reduced to 160 MPa and 3.25%, respectively, while at 5 wt% ZnO, these values drop to 180 MPa and 1.35%, respectively. This degradation in mechanical performance suggests a reduction in fiber flexibility and an increase in stiffness. The observed behavior can be attributed to the effect of nanoparticle content on fiber crystallinity. Low ZnO loading (≤3 wt%) causes only a slight decrease in crystallinity and orientation due to uniform nanoparticle dispersion. However, higher ZnO contents (≥4 wt%) introduce more pronounced lattice distortion and microvoids, which hinder polymer chain alignment during spinning, lowering both crystallinity and orientation. This structural change weakens intermolecular hydrogen bonding and load transfer efficiency, thereby promoting crack initiation and propagation under tensile loading, leading to premature failure [41]. This mechanical deterioration illustrates a typical colloidal aggregation effect, where loss of interfacial stabilization directly translates into compromised macroscopic properties. Despite the decrease in mechanical properties, the composite fibers retain adequate strength and rigidity to meet the basic mechanical requirements for textile applications. Furthermore, the interplay between crystallinity/orientation and mechanical strength highlights that maintaining uniform ZnO dispersion without excessive aggregation is critical to preserving fiber integrity.

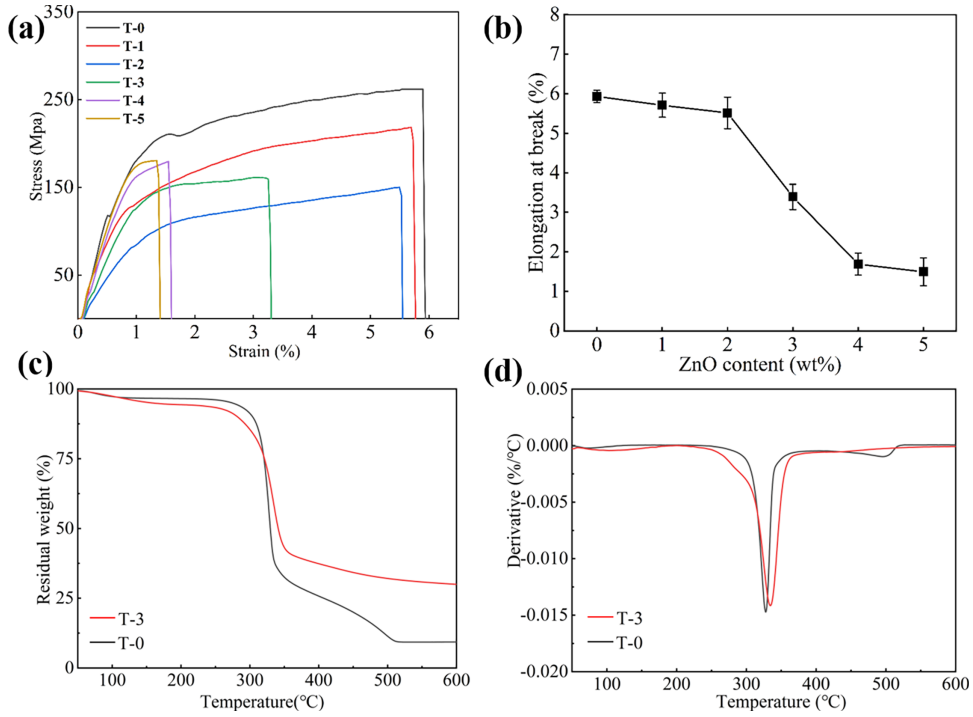

Figure 4: (**a**) Tensile stress–strain curves, (**b**) elongation at break, (**c**) TGA and (**d**) DTG curves of pristine Lyocell and composite fibers.

Fig. 4c,d present the TGA and DTG curves of the pristine fibers (T-0) and the composite fibers (T-3). The thermal degradation of the pristine Lyocell fibers occurs in three main stages. The first stage (100°C–150°C) involves a ~4% mass loss, attributed to evaporation of adsorbed moisture. The second stage (285°C–400°C) shows the main degradation with a maximum rate at 327°C, accounting for ~71% mass loss, corresponding to glycosidic linkage breakdown, pyranose ring opening, and volatile release (CO, CO_2, aldehydes). The third stage (>400°C) involves gradual decomposition of residual char, leaving ~9% residue at 600°C.

For T-3 fibers, the onset of the second degradation stage is ~270°C, with a peak rate at 334°C and a lower mass loss (~55%) in this range. The residual mass at 600°C increases to ~30%, comprising carbonaceous char, ZnO, and other inorganics. These findings demonstrate that the incorporation of ZnO enhances the thermal stability of the composite fibers, which is advantageous for maintaining their structural integrity and performance under elevated temperatures in practical textile applications [42].

3.3 Antibacterial Performance Analysis

Fig. 5a presents the antibacterial performance of ZnO/Lyocell fibers with colony counting method using pristine Lyocell fibers as control. The ZnO/Lyocell fibers exhibit strong antibacterial activity against both *E. coli* and *S. aureus*. Specifically, T-1 fibers achieved antibacterial rates of 83.5% and 85.0% against *E. coli* and *S. aureus*, respectively. For T-3 fibers, the antibacterial rates significantly increase to 96.1% and 95.1%, As the ZnO content continuously increased, the antibacterial performance slowly increase. For T-5 fibers, the inhibition rate reaches 98.0% against both bacterial strains. The above results can be clearly demonstrated by Fig. 5c. A comparison with recent literature (Table S2) indicates that the antibacterial performance of the present ZnO/Lyocell composite fibers is comparable to or higher than that of most reported inorganic antimicrobial fiber systems, highlighting the competitiveness of the proposed strategy. Considering morphology, mechanical strength, antibacterial effect, as well as cost, 3 wt% addition content of rod-shape ZnO nanoparticle is the optimal for antibacterial modification for Lyocell fiber.

Fig. 5b,d illustrate the antibacterial durability of the composite fibers (T-3) after multiple washing cycles. As the number of washing cycles increase, the antibacterial activity shows a slight decline. Nevertheless, even after 50 laundering cycles, the composite fibers retain inhibition rates above 80% against both *S. aureus* and *E. coli*.

This exceptional durability can be attributed to the robust interfacial anchoring of ZnO nanorods within the cellulose matrix, achieved through the PEG-assisted stabilization strategy. Beyond dispersion, the PEG layer also serves as a molecular bridge between ZnO and cellulose. Its terminal hydroxyl groups form additional hydrogen bonds with Lyocell, improving interfacial compatibility and firmly anchoring the nanorods within the matrix. This robust integration minimizes ZnO leaching during washing and underpins the excellent laundering durability. These results demonstrate that the dry-jet wet spinning process, combined with PEG-mediated surface engineering, imparts Lyocell fibers with durable antibacterial functionality, making them highly suitable for repeated use in practical textile applications. Supplementary experiments further confirm that light irradiation plays a critical role in enhancing antibacterial efficiency through ROS generation, while environmental humidity (30% and 80% RH) has a negligible influence on antibacterial performance (Fig. S3).

The antibacterial activity of the composite fibers was further assessed using the inhibition zone assay, as shown in Fig. S4. Filter paper discs thoroughly impregnated with the ZnO/Lyocell fibers were placed on agar plates inoculated with *E. coli* and *S. aureus*. After incubation, clear inhibition zones are observed around all discs, confirming their antibacterial activity. However, the inhibition zones are relatively small, indicating moderate antibacterial efficacy. This limited zone of inhibition is likely attributed to the antibacterial mechanism of ZnO, which does not primarily rely on the release and diffusion of Zn^{2+} ions into the surrounding medium. Instead, antibacterial action is mainly achieved through the generation of ROS catalyzed by ZnO [43,44]. To verify this hypothesis, complementary experiments will be performed in subsequent studies to substantiate this viewpoint. which acts locally on the fiber surface to inactivate bacteria. Furthermore, the inherently low solubility of ZnO in neutral aqueous environments restricts the release of Zn^{2+} ions, thereby limiting its diffusional antibacterial effect in the agar medium [45]. This localized surface-driven mechanism is consistent with colloidal surface reactivity models, where catalytic activity is

governed by surface defect states and interfacial electron transfer. Notably, the size of the inhibition zones remains stable with extended incubation, indicating sustained and consistent antibacterial performance of the composite fibers during the testing period. These results suggest that the composite fibers can effectively suppress the growth of both *E. coli* and *S. aureus* through a contact-based antibacterial mechanism rather than ion-mediated diffusion.

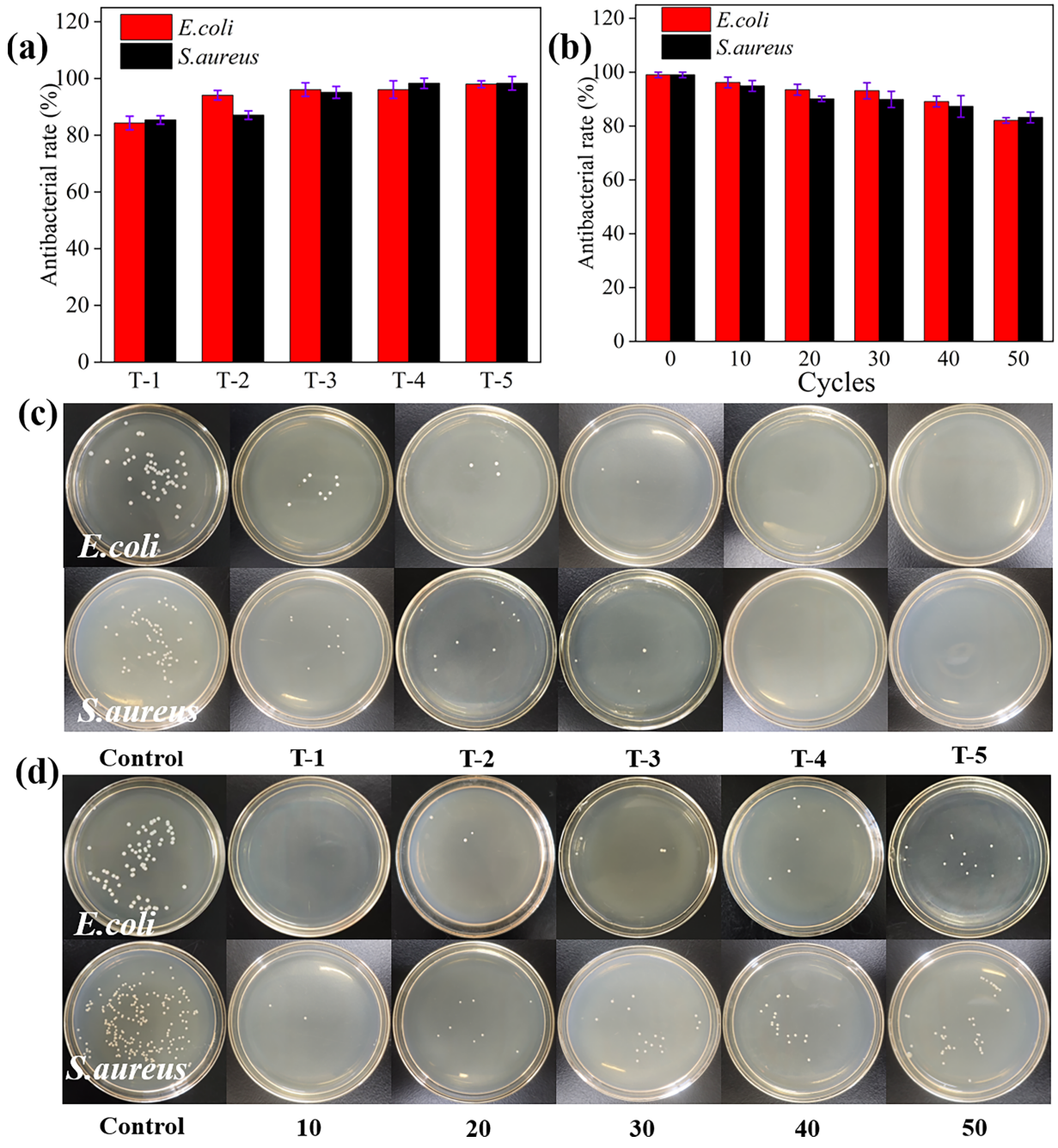

Figure 5: (**a**) Antibacterial rates of composite fibers with different ZnO contents, (**b**) Antibacterial durability after repeated washing (T-3), (**c**) Photos of antibacterial tests at varying ZnO loadings, (**d**) Antibacterial performance after 10–50 washing cycles (T-3).

The antibacterial effect of the 3%-ZnO/Lyocell was further visualized by live/dead bacterial staining method, as shown in Fig. 6. Green-fluorescent nucleic acid dye SYTO9 can penetrate intact bacterial cell membranes, bind to nucleic acids, and emit green fluorescence under blue light excitation. In contrast, propidium iodide (PI) cannot pass through intact membranes but can penetrate compromised membranes and bind to nucleic acids, emitting red fluorescence under blue light. This dual staining method was employed to assess bacterial viability. In the blank control group for *E. coli*, intense green fluorescence indicates high bacterial viability. In contrast, *E. coli* treated with 3%-ZnO/Lyocell exhibits predominantly red fluorescence and significantly reduced green fluorescence, reflecting a marked decrease in cell viability.

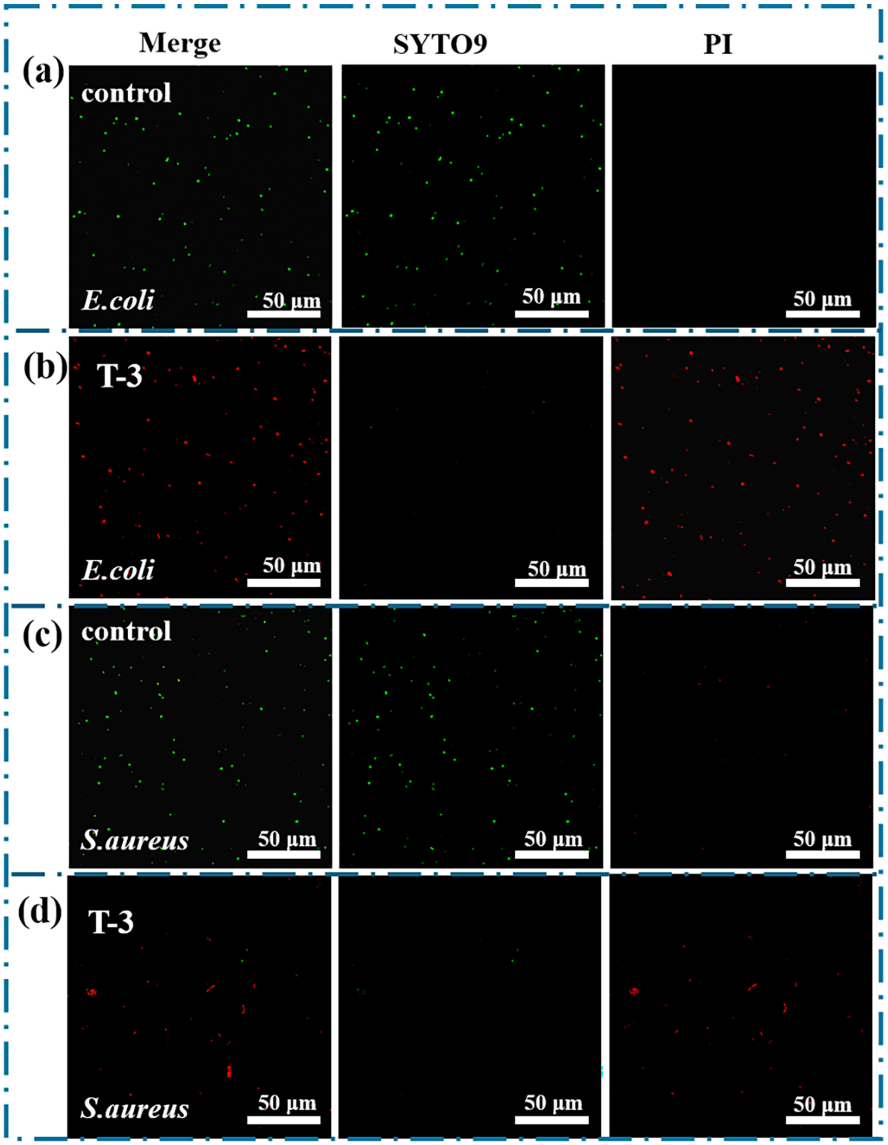

Figure 6: Fluorescence images of live and dead *S. aureus* and *E. coli* in the control group (**a**,**c**) and the composite fibers (T-3) group (**b**,**d**).

A similar trend was observed for *S. aureus*. The control group displays strong green fluorescence and limited red fluorescence, suggesting good bacterial survival. However, upon exposure to the composite fibers, *S. aureus* cells show a predominance of red fluorescence with minimal green fluorescence, confirming

extensive bacterial membrane damage and cell death. These results further corroborate the strong antibacterial efficacy of the ZnO/Lyocell composite fibers, consistent with the findings from quantitative assays.

3.4 Mechanism Analysis

To further elucidate the antibacterial mechanism of ZnO/Lyocell fibers, morphological changes of *E. coli* and *S. aureus* were examined using SEM and TEM, as shown in Fig. 7. In the untreated control group, both *E. coli* and *S. aureus* exhibit intact cell morphology with smooth and well-defined surfaces (Fig. 6a,c,e,g). However, following exposure to the composite fibers (T-3), the bacterial cells displayed noticeable morphological damage, including membrane deformation, surface collapse, and structural disruption, indicating compromised cell integrity (Fig. 7b,d,f,h).

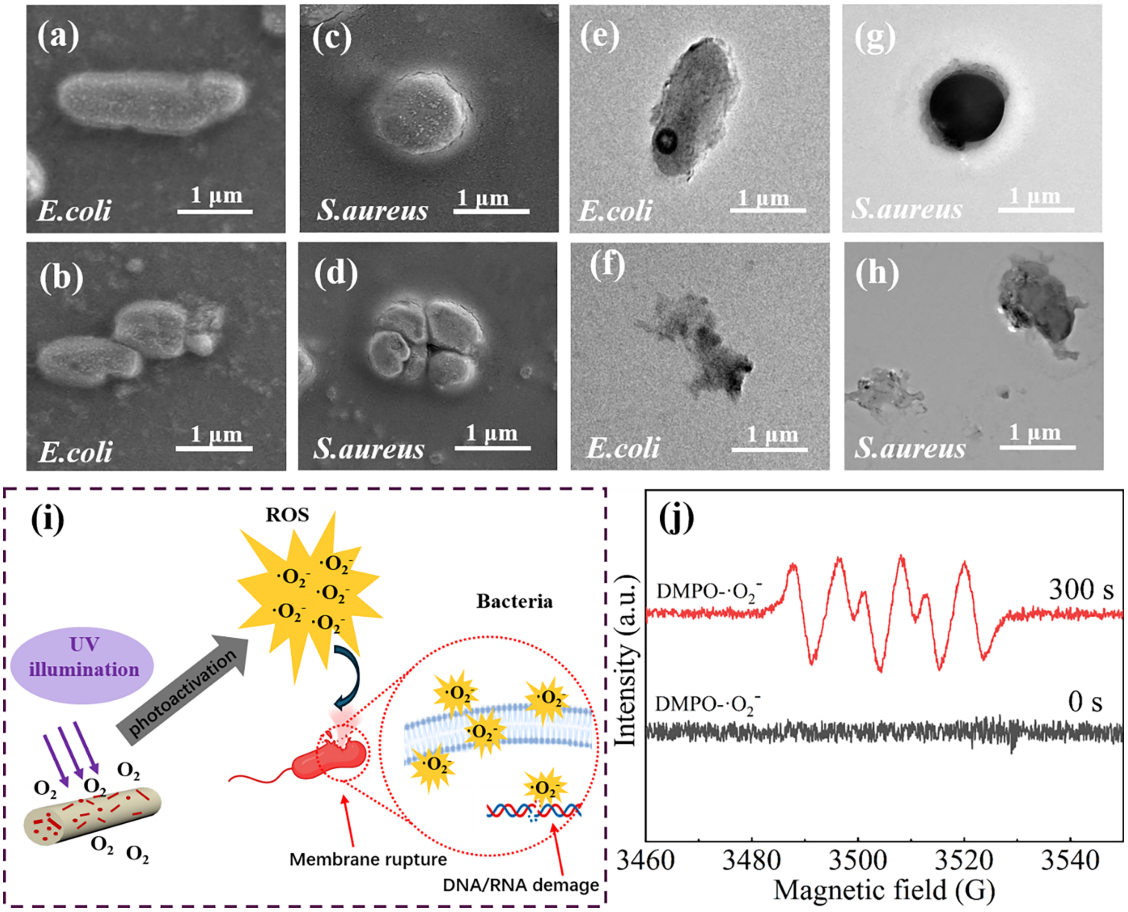

Figure 7: SEM and TEM images of *E. coli* and *S. aureus* before (**a**,**c**,**e**,**g**) and after treatment with the T-3 composite fiber (**b**,**d**,**f**,**h**). (**i**) Schematic illustration of the proposed antibacterial mechanism of the ZnO/Lyocell composite. (**j**) EPR spectra for DMPO- $\cdot O^{2-}$ at methanol solution for T-3.

Based on these observations, a plausible antibacterial mechanism is proposed, as illustrated in Fig. 7i. ZnO nanorods are identified as the primary antibacterial agents in the composite fibers. Under aerobic and light irradiation conditions, ZnO located on the fiber surface catalytically generates reactive oxygen species (ROS), which induce oxidative damage to bacterial cell membranes and intracellular components [46]. Importantly, PEG-mediated stabilization preserves the nanoscale rod-like morphology and defect-rich surfaces of ZnO nanorods, which serve as active sites for ROS generation. By suppressing nanoparticle

aggregation, PEG maintains a high accessible surface area and promotes efficient adsorption of oxygen and water molecules, thereby enhancing ROS production, as evidenced by the characteristic EPR signals shown in Fig. 7j. Specifically, no DMPO–•O_2^- signal was detected in the absence of light irradiation, whereas a distinct quadruple peak with an intensity ratio of 1:2:2:1 appeared after 300 s of light exposure, confirming effective ROS generation under illumination [47]. To further elucidate the dominant antibacterial pathway, control experiments conducted under dark conditions reveal a pronounced decrease in antibacterial efficiency (Fig. S3), indicating that light-induced ROS generation plays a primary role in bacterial inactivation. Nevertheless, the residual antibacterial activity observed in the dark suggests that Zn^{2+} release provides a secondary contribution. Overall, the antibacterial performance of the ZnO/Lyocell composite fibers originates from the synergistic effect of photocatalytically generated ROS and Zn^{2+}-related antibacterial action, with ROS being the dominant contributor. Therefore, antibacterial efficacy is governed not only by ZnO loading, but more critically by dispersion quality and interfacial accessibility. PEG functionalization thus plays a dual role by simultaneously improving ZnO dispersion and stabilizing the solid–liquid interface, thereby preserving photocatalytic activity and translating nanoscale colloidal stability into durable antibacterial performance.

4 Conclusion

In summary, this study presents a PEG-assisted colloidal stabilization strategy for rod-shaped ZnO nanorods and demonstrates its successful application in fabricating antibacterial Lyocell fibers via dry-jet wet spinning. The PEG molecules adsorbed on ZnO nanorod surfaces provided steric stabilization, which effectively prevented aggregation and enabled uniform dispersion within the cellulose matrix. This interfacial engineering approach ensured both enhanced antibacterial efficacy and superior durability. Specifically, incorporation of 3 wt% ZnO achieved a balance between antibacterial efficiency and mechanical performance, delivering inhibition rates above 95% against *E. coli* and *S. aureus*, while retaining over 80% efficacy even after 50 laundering cycles.

Mechanistic investigations further confirm that ROS generation under light irradiation plays a dominant role in bacterial inactivation, whereas Zn^{2+} release contributes as a secondary antibacterial pathway. Moreover, the antibacterial performance exhibits minimal dependence on environmental humidity, highlighting the robustness of the composite fibers under practical service conditions. Beyond textile applications, this work underscores the broader importance of colloidal stabilization in nanomaterial–polymer composites. The PEG-assisted dispersion strategy provides a generalizable framework for addressing colloidal instability of anisotropic nanoparticles and offers insights into interfacial design principles for developing advanced functional materials.

Acknowledgement: Not applicable.

Funding Statement: This work was supported by the Key Research and Development Plan Project of Hubei Province (No. 2022BAD009); the National Natural Science Foundation of China (No. 51504168), and the Hubei Province key research and development (R&D) plan projects (2025BAB005).

Author Contributions: The authors confirm contribution to the paper as follows: Conceptualization, Peiyu Cui, Xiaobo Ye, Bin Fang and Yimin Sun; methodology, Biao Liu, Junlong Yao and Yimin Sun; software, Zexin Lin; formal analysis: Biao Liu and Xin Wei; investigation, Biao Liu and Xin Wei; resources, Peiyu Cui; data curation, Xin Wei and Zexin Lin; writing-original draft, Biao Liu; writing—review & editing, Yani Guo and Yimin Sun; visualization: Biao Liu and Peiyu Cui; supervision: Yani Guo and Yimin Sun; project administration, Bin Fang; funding acquisition: Xiaobo Ye. All authors reviewed and approved the final version of the manuscript.

Availability of Data and Materials: Data available on request from the authors.

Ethics Approval: Not applicable.

Conflicts of Interest: The authors declare no conflicts of interest.

Supplementary Materials: The supplementary material is available online at https://www.techscience.com/doi/10.32604/jpm.2026.077831/s1.

References

1. Jiang X, Bai Y, Chen X, Liu W. A review on raw materials, commercial production and properties of lyocell fiber. J Bioresour Bioprod. 2020;5(1):16–25. doi:10.1016/j.jobab.2020.03.002.
2. Sayyed AJ, Deshmukh NA, Pinjari DV. A critical review of manufacturing processes used in regenerated cellulosic fibres: viscose, cellulose acetate, cuprammonium, LiCl/DMAc, ionic liquids, and NMMO based lyocell. Cellulose. 2019;26(5):2913–40. doi:10.1007/s10570-019-02318-y.
3. Sawiak M, Souto BA, Lawson L, Lo J, Dolez PI. Recovery of N-methylmorpholine N-oxide (NMMO) in lyocell fibre manufacturing process. Fibers. 2025;13(1):3. doi:10.3390/fib13010003.
4. He Y, Cao Z, Deng C, Zheng L, Xu J, Zhang Z, et al. Sustainable and efficient strategy for functional Lyocell fiber manufacture through curcumin-loaded nanospheres. Ind Crops Prod. 2024;222:119908. doi:10.1016/j.indcrop.2024.119908.
5. Yang G, Zhou Y, Zhang H, Wang S, Yao X, Shao H. Preparation and characterization of dissolving pulp and lyocell fibers from corncob. Cellulose. 2023;30(8):4841–53. doi:10.1007/s10570-023-05179-8.
6. Edgar KJ, Zhang H. Antibacterial modification of Lyocell fiber: A review. Carbohydr Polym. 2020;250(1):116932. doi:10.1016/j.carbpol.2020.116932.
7. Shen D, Chen L, Wu S, Chen K, Qi D, Zhu S. Fibrillation in cellulose-based Lyocell: chemical insights, engineering solutions and emerging challenges. Carbohydr Polym. 2025;363(14):123722. doi:10.1016/j.carbpol.2025.123722.
8. Deng Y, Si Y, Sun G. Fibrous materials for antimicrobial applications. In: Handbook of fibrous materials. Hoboken, NJ, USA: Wiley; 2020. p. 927–51. doi:10.1002/9783527342587.ch33.
9. He C, Yuan L, Bi S, Zhou C, Yang Q, Gu J, et al. Modified chitosan-based coating/packaging composites with enhanced antibacterial, antioxidant, and UV-resistant properties for fresh food preservation. ACS Appl Mater Interfaces. 2024;16(36):48352–62. doi:10.1021/acsami.4c10643.
10. Jøraholmen MW, Bhargava A, Julin K, Johannessen M, Škalko-Basnet N. The antimicrobial properties of chitosan can be tailored by formulation. Mar Drugs. 2020;18(2):96. doi:10.3390/md18020096.
11. Li W, Li H, Shi Q, Sun T, Xie X, Song B, et al. The dynamics and mechanism of the antimicrobial activity of tea tree oil against bacteria and fungi. Appl Microbiol Biotechnol. 2016;100(20):8865–75. doi:10.1007/s00253-016-7692-4.
12. Kumar S, Kalita S, Basumatary IB, Kumar S, Ray S, Mukherjee A. Recent advances in therapeutic and biological activities of Aloe vera. Biocatal Agric Biotechnol. 2024;57(7):103084. doi:10.1016/j.bcab.2024.103084.
13. Abou El Fadl FI, Hegazy DE, Maziad NA, Ghobashy MM. Effect of nano-metal oxides (TiO_2, MgO, CaO, and ZnO) on antibacterial property of (PEO/PEC-co-AAm) hydrogel synthesized by gamma irradiation. Int J Biol Macromol. 2023;250(7):126248. doi:10.1016/j.ijbiomac.2023.126248.
14. Tamilselvi R, Kalaiarasi M, Elumalai M, Malarkodi T, Venkatesh A, Venkatachalam P. Antimicrobial activity of metal oxide nanoparticles. Biomed Pharmacol J. 2024;17:1757–67. doi:10.1016/j.msec.2014.08.031.
15. Jin Z, Li J, Zhang Y, Liu D, Ding H, Mamba BB, et al. Rational design of efficient visible-light photocatalysts (1D@2D/0D) ZnO@ Ni-doped BiOBr/Bi heterojunction: considerations on hierarchical structures, doping and SPR effect. J Mater Sci Technol. 2022;125:38–50. doi:10.1016/j.jmst.2022.01.034.
16. Raub AAM, Bahru R, Nashruddin SNAM, Yunas J. A review on vertical aligned zinc oxide nanorods: synthesis methods, properties, and applications. J Nanopart Res. 2024;26(8):186. doi:10.1007/s11051-024-06098-w.
17. Rutherford D, Jíra J, Kolářová K, Matolínová I, Mičová J, Remeš Z, et al. Growth inhibition of gram-positive and gram-negative bacteria by zinc oxide hedgehog particles. Int J Nanomed. 2021;16:3541–54. doi:10.2147/IJN.S300428.

18. Cao C, Zhang B, Lin S. p-type ZnO for photocatalytic water splitting. APL Mater. 2022;10(3):030901. doi:10.1063/5.0083753.
19. Loh KP, Chua SJ. Zinc oxide nanorod arrays: Properties and hydrothermal synthesis. In: Molecular building blocks for nanotechnology. Berlin/Heidelberg, Germany: Springer; 2007. p. 92–117. doi:10.1007/978-0-387-39938-6_6.
20. Zheng S, Chen W, Shi C, Han J. Thermostable ZnO/Ag@SiO_2 nanohybrid material for extraordinary antibacterial activity polyester fibers. Polym Eng Sci. 2024;64(1):386–98. doi:10.1002/pen.26555.
21. Kim DY, Lee JB, Lee DY. Selective localization of nanofiller on mechanical properties of poly (lactic acid)/poly (butylene adipate-co-terephthalate) nanocomposites via the surface energy and melt blending technique. Macromolecules. 2022;55(8):3287–300. doi:10.1021/acs.macromol.1c02074.
22. Soni SK, Thomas B, Thomas SB, Tile PS, Sakharwade SG. Carbon nanotubes as exceptional nanofillers in polymer and polymer/fiber nanocomposites: an extensive review. Mater Today Commun. 2023;37:107358. doi:10.1016/j.mtcomm.2023.107358.
23. Wang P, Jiang Y, Liu X, Yu K, Qian K, Zhang Z. Study on the mechanical properties of shear thickening fluid-filled polyurethane foam composites. Mater Res Express. 2020;6(12):125380. doi:10.1088/2053-1591/ab5f98.
24. Yang W, Xu J, Niu L, Zhao J, Wang C, Liu X. Dispersion stability of nano-Sb2O3 particles modified with polyethylene glycol. Part Sci Technol. 2018;36(7):844–9. doi:10.1080/02726351.2017.1305027.
25. Zhu QW, Ou MG. The function of PEG in the synthesis of nanomaterials. Appl Mech Mater. 2014;670:3–6. doi:10.4028/www.scientific.net/AMM.670-671.3.
26. Zhang R, Tang L, Ji X, Su Y, Xu N, Feng Y, et al. Continuous preparation and antibacterial mechanisms of biodegradable polylactic acid/nano-zinc oxide/additives antibacterial non-wovens. Int J Biol Macromol. 2024;269(1):132188. doi:10.1016/j.ijbiomac.2024.132188.
27. Zhang G, Xiao Y, Yan J, Xie N, Liu R, Zhang Y. Ultraviolet light-degradation behavior and antibacterial activity of polypropylene/ZnO nanoparticles fibers. J Mater Sci Technol. 2019;11(11):1841. doi:10.3390/polym11111841.
28. Alameen AS, Yaseen SA, Saif FA, Undre SB, Undre PB. Intermolecular interactions of ZnO nanodispersion with aqueous polyethylene glycol via physicochemical and optical study. Bull Mater Sci. 2022;45(3):153. doi:10.1007/s12034-022-02721-5.
29. Chruściel JJ, Olczyk J, Kudzin MH, Kaczmarek P, Król P, Tarzyńska N. Antibacterial and antifungal properties of polyester, polylactide, and cotton nonwovens and fabrics, by means of stable aqueous dispersions containing copper silicate and some metal oxides. Materials. 2023;16(16):5647. doi:10.3390/ma16165647.
30. Barkhade T, Nigam K, Ravi G, Rawat S, Nema SK. Investigating the effects of microwave plasma on bacterial cell structures, viability, and membrane integrity. Sci Rep. 2025;15(1):18052. doi:10.1038/s41598-025-02312-4.
31. Annisa R, Fauziyah B, Megawati DS, Zahrah F. Formulation of silver nanoparticle mouthwash and testing of antibacterial activity against *Staphylococcus aureus*. J Trop Pharm Chem. 2023;7(2):52–8. doi:10.25026/jtpc.v7i2.386.
32. Wu R, Li C, Li J, Sjollema J, Geertsema-Doornbusch GI, de Haan-Visser HW, et al. Bacterial killing and the dimensions of bacterial death. npj Biofilms Microbiomes. 2024;10(1):87. doi:10.1038/s41522-024-00559-9.
33. Folorunso O, Kumar N, Hamam Y, Sadiku R, Ray SS. Facile solvent/drying fabrication of PVA/PPy/rGO:A novel nanocomposite for energy storage applications. Results Mater. 2022;15(2):100295. doi:10.1016/j.rinma.2022.100295.
34. Li X, Deng L, Li Y, Li K. Preparation of microcrystalline cellulose from bagasse bleached pulp reinforced polylactic acid composite films. Sugar Tech. 2020;22(6):1138–47. doi:10.1007/s12355-020-00827-w.
35. Alwesabi WA, Dange PD, Raut AV, Puri GM, Khobragade RM, Pawar PP, et al. Microstructural, optical, and antimicrobial activity of ZnO-CuO NCP prepared using co-precipitation technique. J Supercond Nov Magn. 2024;37(11-12):1923–37. doi:10.1007/s10948-024-06760-3.
36. Li H, Zhang L, Lu H, Ma J, Zhou X, Wang Z, et al. Macro-/nanoporous Al-doped ZnO/cellulose composites based on tunable cellulose fiber sizes for enhancing photocatalytic properties. Carbohydr Polym. 2020;250:116873. doi:10.1016/j.carbpol.2020.116873.
37. Petrushenko SI, Fijalkowski M, Kopach VR, Shepotko YM, Adach K, Dukarov SV, et al. Triboelectric nanogenerators based on nanostructured Layers of zinc oxide deposited on carbon fabric. J Compos Sci. 2023;7(12):496. doi:10.3390/jcs7120496.

38. Dutta S, Chattopadhyay S, Sarkar A, Chakrabarti M, Sanyal D, Jana D. Role of defects in tailoring structural, electrical and optical properties of ZnO. Prog Mater Sci. 2009;54(1):89–136. doi:10.1016/j.pmatsci.2008.07.002.
39. Chris JB, Ambroise C, Daniel RJ, Aled RL, Lewys JJ, Richard JC, et al. XPS investigation of titanium contact formation to ZnO nanowires. Nanotechnol. 2017;28(8):085301. doi:10.1088/1361-6528/aa5663.
40. Li Z, Xiong Y, Xie Y. Selected-control synthesis of ZnO nanowires and nanorods via a PEG-assisted route. Inorg Chem. 2003;42(24):8105–9. doi:10.1021/ic034029q.
41. Onyszko M, Marko Ywska-Szczupak A, Rakoczy R, Paszkiewicz O, Janusz J, Gorgon-Kuza A, et al. The cellulose fibers functionalized with star-like zinc oxide nanoparticles with boosted antibacterial performance for hygienic products. Sci Rep. 2022;12(1):1321. doi:10.1038/s41598-022-05458-7.
42. Feng B, Ren Y, Shi L, Xue Z, Li X, Xiao Z, et al. Efficient anti-fibrillation of lyocell fabric by low-formaldehyde resin. Ind Crops Prod. 2024;213:118406. doi:10.1016/j.indcrop.2024.118406.
43. Chandrasekaran K, Bathula C. 3d-marigold-like barium-modified zinc oxide for antibacterial and anticancer studies. Ceram Int. 2024;50(9):15333–9. doi:10.1016/j.ceramint.2024.01.382.
44. Joe A, Park SH, Kim DJ, Lee YJ, Jhee KH, Sohn Y, et al. Antimicrobial activity of ZnO nanoplates and its Ag nanocomposites: insight into an ROS-mediated antibacterial mechanism under UV light. J Solid State Chem. 2018;267:124–33. doi:10.1016/j.jssc.2018.08.003.
45. Amelia SR, Rohmatulloh Y, Listiani P, Devi MJ, Ichikawa Y, Honda M, et al. One pot synthesis and performance of N-and (Mg, B, N)-doped ZnO for photocatalytic and antibacterial applications: experimental and theoretical investigations. Ceram Int. 2024;50(7):11216–35. doi:10.1016/j.ceramint.2024.01.023.
46. Amin YA, Abdelaziz SG, Said AH. Treatment of postpartum endometritis induced by multidrug-resistant bacterial infection in dairy cattle by green synthesized zinc oxide nanoparticles and *in vivo* evaluation of its broad spectrum antimicrobial activity in cow uteri. Res Vet Sci. 2023;165:105074. doi:10.1016/j.rvsc.2023.105074.
47. Haitosa HH, He L, Chen P, Kabtamu DM, Zelekew OA, Wu Y. Visible-light-driven Fe-doped UiO-66-NH_2@CuO p-n heterojunctions: synergistic photo-fenton catalysis for sustainable water remediation. J Environ Chem Eng. 2025;13(6):120296. doi:10.1016/j.jece.2025.120296.